Transformer Integrated With Additional Resonant Inductor for Phase-Shift Full-Bridge Converter With Primary Clamping Diodes

Kyu-Min Cho, *Student Member, IEEE*, Young-Do Kim, *Student Member, IEEE*, In-Ho Cho, *Student Member, IEEE*, and Gun-Woo Moon, *Member, IEEE*

***Abstract*—A new transformer integrated with additional resonant inductor is proposed in this paper. By winding on outer side of transformer, the proposed transformer can implement the additional resonant inductor without extra magnetic component. As a result, it can reduce cost and core loss due to the additional resonant inductor. In addition, it can adopt primary clamping diodes to reduce the voltage ringing of secondary rectifiers, although the additional resonant inductor and the transformer are integrated physically. Experimental result of 1200 W (12 V, 100 A) prototype shows that the phase-shift full-bridge converter incorporated with proposed transformer can achieve high efficiency and low cost.**

***Index Terms*—Additional resonant inductor, phase-shift full-bridge (PSFB) converter, transformer.**

I. Introduction

THE PHASE-SHIFT full-bridge (PSFB) converter is a very attractive topology for high-power applications because of its desired advantages, such as low current/voltage stress of semiconductor components, zero dc offsets of magnetizing current, and zero-voltage switching (ZVS) of all switches by utilizing the transformer's leakage inductor and the intrinsic capacitor of switches [1]–[5]. However, the transformer's leakage inductor is determined by various physical factors, such as air-gap, core material, core shape, winding method, etc., thus it is difficult to estimate/design its value. As a result, the additional resonant inductor is widely used in the practical applications. Although it is simple and can easily guarantee desired ZVS ranges by adjusting its value, it causes severe voltage ringing across secondary rectifiers (SRs) due to the energy stored in it.

To overcome these drawbacks, various methods have been proposed [6]–[10]. Among them, the PSFB converter proposed in [9] can effectively reduce the voltage ringing across SRs using primary clamping diodes, as shown in Fig. 1. After commutation is finished, the voltage across SRs is increased by the resonance between the intrinsic capacitor of SRs and the total resonant inductor, such as the sum of transformer's leakage inductor and additional resonant inductor. When the reflected primary voltage of transformer reaches the input voltage, clamping diode is turned ON. Concurrently, the additional resonant inductor is shorted through clamping diode and lagging leg switch. Therefore, the energy stored in additional resonant inductor is separated from the resonant mechanism, which results in low voltage ringing across SRs.

In general, the core loss of magnetic components can be easily calculated under sinusoidal excitation [11], [12]. However, square-wave voltage with small duty ratio applies to the additional resonant inductor because the primary side of transformer is shorted during a short commutation period, as shown in Fig. 1(b). As a result, nonsinusoidal excitation occurs in the additional resonant inductor. As well known, the core loss of magnetic components is affected by frequency, flux density variation, and applied voltage waveforms [13]–[17]. Especially, when square-wave voltage applies to magnetic components, its core loss is dramatically increased in inverse proportion to its duty ratio [13]. Therefore, the additional resonant inductor has high core loss and bulky size compared with its handling power.

To overcome these problems, this paper proposes a new transformer integrated with additional resonant inductor. As shown in Fig. 2(b), by winding on outer side of transformer, the proposed transformer implements the additional resonant inductor without extra magnetic component. Therefore, it can eliminate cost and size problems due to the additional resonant inductor. In addition, it can achieve low core loss by utilizing large air-gap and large cross-section area. The review of the core loss, operational principle, design considerations, and experimental results are presented to confirm the validity of the proposed transformer.

II. Proposed Transformer

A. Review of the Core Loss of Additional Resonant Inductor

Generally, the core loss of magnetic components can be calculated using a Steinmetz equation (SE) as follows:

$$P_{v\_\mathrm{SE}} = \kappa f^{\alpha} \Delta B^{\beta} \tag{1}$$

where P_{v_SE} is the core loss per unit volume using SE, ΔB is the peak flux amplitude, f is the frequency of the sinusoidal

Manuscript received February 17, 2010; revised May 3, 2010, August 24, 2010, and November 14, 2010; accepted December 27, 2010. Date of current version February 27, 2012. This paper was presented in part at the Energy Conversion Congress and Exposition, San Jose, CA, September 2009. Recommended for publication by Associate Editor J. A. Cobos.

The authors are with Department of Electrical Engineering, Korea Advanced Institute of Science and Technology, Daejeon 305–701, Korea (e-mail: negative@angel.kaist.ac.kr, nemind@angel.kaist.ac.kr, inhara@angel.kaist.ac.kr, gwmoon@ee.kaist.ac.kr)

Color versions of one or more of the figures in this paper are available online at http://ieeexplore.ieee.org.

Digital Object Identifier 10.1109/TPEL.2011.2106514

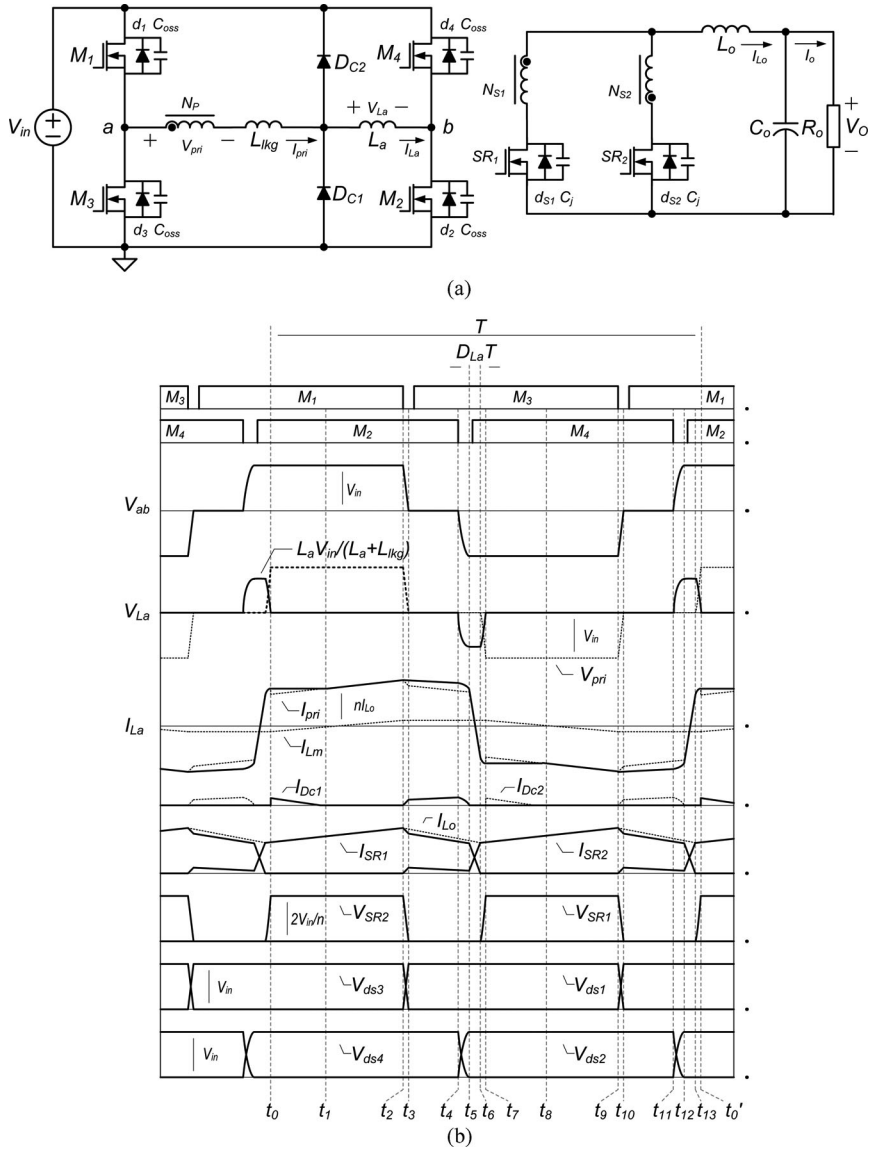

Fig. 1. Conventional PSFB converter with primary clamping diodes. (a) Circuit diagram. (b) Key waveforms.

excitation, and κ, $\alpha(=1, 2)$, and $\beta(=2, 3)$ are empirical parameters, which are usually given by manufacture.

It has proven to be the most useful equation for the calculation of core loss under sinusoidal excitation. However, it cannot explain that the core loss is increased under nonsinusoidal excitation. To solve this problem, various approaches have proposed [13]–[17]. Among them, the modified SE (MSE) can calculate core loss under nonsinusoidal excitation by defining the equivalent frequency [15]. Base on the MSE, the equivalent frequency $f_{\rm eq}$ and the core loss of additional resonant inductor per unit volume $P_{v\_{\rm MSE}}$ can be expressed as follows:

$$f_{\rm eq} = \frac{2}{\pi^2 (2\Delta B)^2} \int_0^{1/f} \left(\frac{dB}{dt}\right)^2 dt \tag{2}$$

$$P_{v\_{\rm MSE}} = \kappa f_{\rm eq}^{\alpha-1} \Delta B^{\beta} f. \tag{3}$$

Assuming that most of dB/dt occurs during t_5–t_6 for the convenience of analysis, ΔB and dB/dt of the additional resonant inductor can be expressed as follows:

$$\Delta B = \frac{2L_a I_o}{nNA} \tag{4}$$

$$\frac{dB(t)}{dt} = \begin{cases} 0, & t_0 < t \le t_5 \\ \dfrac{1}{NA}\dfrac{L_a}{L_a + L_{\rm lkg}} V_{\rm in}, & t_5 < t \le t_5 + D_{L_a} T \\ 0, & t_6 < t \le t_{12} \\ -\dfrac{1}{NA}\dfrac{L_a}{L_a + L_{\rm lkg}} V_{\rm in}, & t_{12} < t \le t_{12} + D_{L_a} T \\ 0, & t_{13} < t \le t_0' \end{cases} \tag{5}$$

where L_a is the additional resonant inductance, I_o is the output current, n ($= N_p/N_{S1} = N_p/N_{S2}$) is transformer turn ratios, N is the number of turns, A is the cross-section area, $V_{\rm in}$ is the

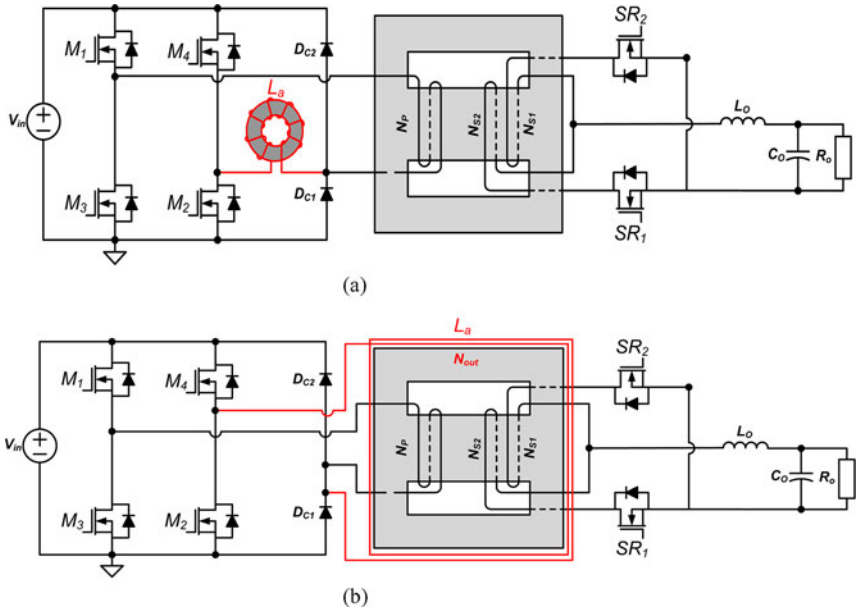

Fig. 2. Proposed transformer integrated with additional resonant inductor. (a) Conventional additional resonant inductor and transformer. (b) Proposed transformer integrated with additional resonant inductor.

input voltage, $L_{\rm lkg}$ is transformer's leakage inductance, T is the switching period, and D_{L_a} is the time period of t_5–t_6.

By substituting (2), (4), and (5) into (3), $P_{v\_\rm MSE}$ can be expressed as follows:

$$P_v\_\rm MSE = \kappa \left(\frac{4f}{\pi^2 D_{La}}\right)^{\alpha-1} \left(\frac{L_a I_o}{nNA}\right)^{\beta} f \qquad (6)$$

where $D_{L_a} = \frac{2(L_a + L_{\rm lkg}) I_o}{n V_{\rm in} T}$.

Fig. 3 shows the core losses using MSE and SE, and their ratios according to the additional resonant inductances. As shown in Fig. 3(a), the additional resonant inductor has high core loss due to the nonsinusoidal excitation. In general, the additional resonant inductor is determined by tradeoff between switching and conduction losses. When large additional resonant inductance is used, it can achieve wide ZVS ranges. However, it causes high conduction loss due to the duty loss, especially at heavy load conditions. By rule of thumb, it is reasonable to design L_a achieving ZVS operations above half-load conditions. In this case, D_{L_a} is from 0.02 to 0.05. Therefore, as shown in Fig. 3(b), the additional resonant inductor has 5–8.5 times higher core loss compared to that calculated with sinusoidal excitation.

From (6), there are two possible approaches to overcome these problems. One is increasing the transformer's leakage inductance and decreasing the additional resonant inductance maintaining D_{L_a}. In this case, it has almost same ZVS ranges due to the same total resonant inductance. Furthermore, it can reduce the core loss of L_a due to small ΔB. However, it causes high voltage ringing of SRs due to the energy stored in large transformer's leakage inductor. The other is the decreasing ΔB with large airgap. When large airgap is used, many turns or large cross-section area is required to implement same additional resonant inductance. As a result, it can achieve the low core loss by small ΔB. However, since bulky magnetic core with large cross-section area or large window area is required, it causes high cost and low power density.

B. Proposed Transformer

To overcome aforementioned problems, a new transformer integrated with the additional resonant inductor is proposed. The proposed transformer implements the additional resonant inductor by winding on outer side of transformer. As shown in Fig. 4(b), primary magnetic flux Φ_p by primary winding N_p creates a change of magnetic flux in the closed current loop by secondary winding N_s. As a result, current/voltage is induced in such a direction to oppose the change of Φ_1, N_p and N_s work as a transformer. However, Φ_p by N_p and $\Phi_{\rm outer}$ by outer winding $N_{\rm out}$ meet at right angle each other, thus $N_{\rm out}$ cannot make any magnetic flux, which appose to Φ_p, Therefore, $N_{\rm out}$ works as the additional resonant inductor with large airgap and large cross-section area.

By implementing the additional resonant inductor utilizing outer side of the transformer, the proposed transformer can achieve several characteristics as follows.

First of all, it requires no extra magnetic component for an additional resonant inductor. Thus, it can achieve low cost. Second, it can easily control the additional resonant inductance by adjusting number of outer turns. Third, since the additional resonant inductor and transformer are separated electrically, it can adopt primary clamping diodes to reduce the voltage ringing of SRs. Fourth, the additional resonant inductor by outer turns can achieve low core loss by utilizing large airgap and large cross-section area. Finally, the proposed transformer has to use ferrite or powder cores. Since the magnetic flux is at right angle to the tape, tape wound core cannot be used.

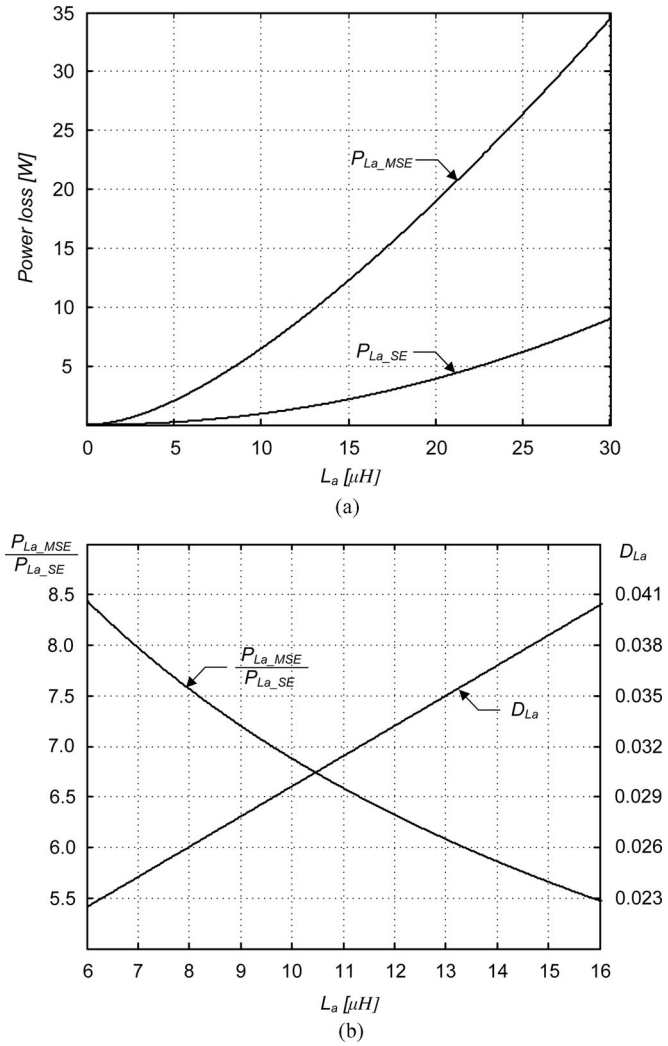

Fig. 3. Core loss of L_a using MSE and SE, and their ratio according to L_a. (a) $P_{L_a\_\mathrm{MSE}}$ and $P_{L_a\_\mathrm{SE}}$. (b) $P_{L_a\_\mathrm{MSE}}/P_{L_a\_\mathrm{SE}}$.

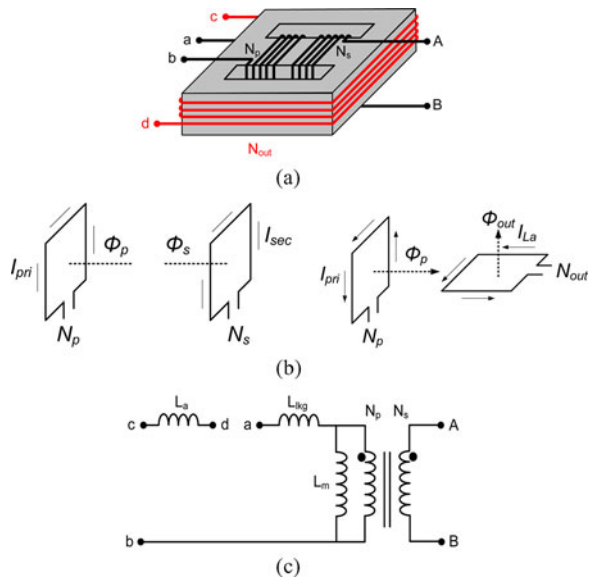

Fig. 4. Proposed transformer. (a) Physical structure. (b) Magnetic fluxes. (c) Equivalent circuit.

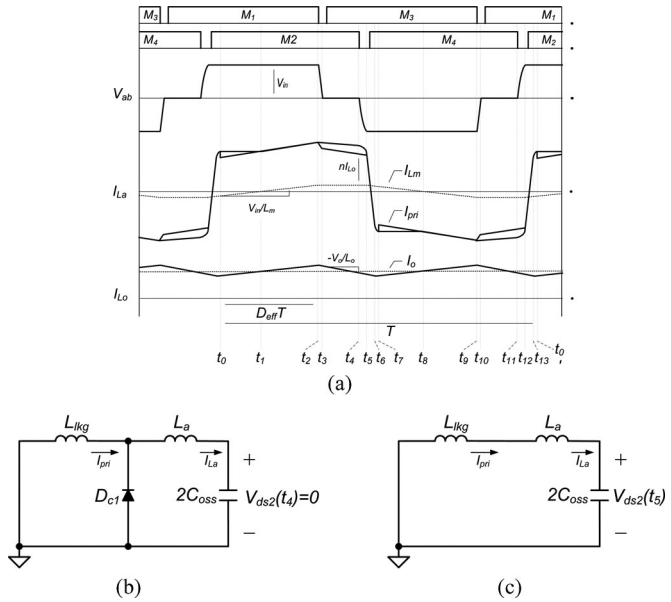

Fig. 5. Key waveforms and equivalent circuits. (a) Key waveforms. (b) Equivalent circuit (t_4–t_5). (c) Equivalent circuit (t_5–t_6).

III. Design Considerations

A. Selection of the Additional Resonant Inductance

Fig. 5 shows the key waveforms and equivalent circuits to calculate ZVS conditions. Since ZVS operations of leading leg switches M_1 and M_3 can be easily achieved by reflected output inductor current, the additional resonant inductance is determined by ZVS conditions of lagging leg switches M_2 and M_4.

After lagging leg switch M_2 is turned OFF at t_4, the primary current I_{pri} freewheels and the additional resonant inductor current I_{L_a} is decreased in a manner of resonance between the additional resonant inductor and intrinsic output capacitors of lagging leg switches, as shown in Fig. 5(b). When I_{L_a} is equal to I_{pri} at t_5, primary clamping diode D_{C1} is turned OFF. At this time, the voltage across switch M_2 can be expressed as follows:

$$V_{ds2}(t_5) = \sqrt{\frac{L_a}{2C_{\mathrm{oss}}}\left(I_{L_a}(t_4)^2 - I_{L_a}(t_5)^2\right)} \tag{7}$$

where

$$I_{L_a}(t_4) = \frac{nV_oT}{4L_m} + \frac{1}{n}\left(I_o + \frac{V_o(1-nV_o/V_{\mathrm{in}})T}{4L_o}\right)$$

$$I_{L_a}(t_5) = \frac{nV_oT}{4L_m} + \frac{1}{n}\left(I_o - \frac{V_o(1-nV_o/V_{\mathrm{in}})T}{4L_o}\right).$$

After t_5, ZVS operation of lagging leg switch M_4 is achieved by the resonance between $L_{\mathrm{lkg}} + L_a$ and $2C_{\mathrm{oss}}$, as shown in Fig. 5(c). Therefore, the energy stored in $L_{\mathrm{lkg}} + L_a$ has to be larger than that stored in $2C_{\mathrm{oss}}$ to achieve ZVS operation of M_4 and it can expressed as follows:

$$\frac{1}{2}(L_{\mathrm{lkg}} + L_a)I_{L_a}(t_5)^2 > \frac{1}{2}(2C_{\mathrm{oss}})(V_{\mathrm{in}} - V_{ds2}(t_5))^2. \tag{8}$$

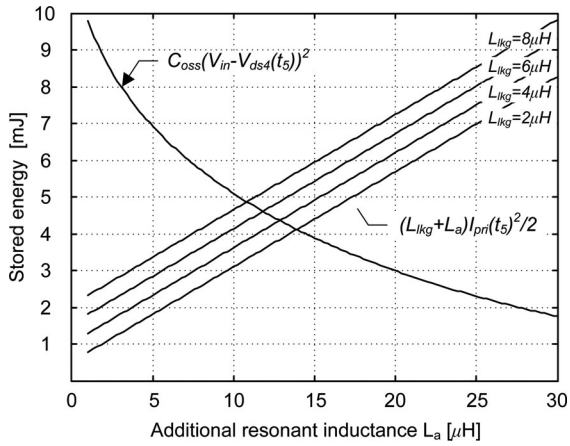

Fig. 6. ZVS conditions at half-load condition.

Fig. 6 shows the ZVS condition at half-load conditions. To achieve ZVS operation, the L_a must have the larger value than 11 μH when $L_{\rm lkg}$ is 6.5 μH.

B. Selection of Number of Outer Turns

The additional resonant inductor of proposed transformer is a kind of rod inductors (see Fig. 7). So far, various methods have been proposed to calculate inductance of a rod inductor [18]–[20]. Among them, the classical expression proposed by Soohoo is simple and had been widely used [18]. However, it was found that it overestimated the actual inductance because of the presence of the demagnetizing filed. Furthermore, it has revealed that inductance by the winding makes a contribution to the total inductance of a rod inductor. Taking these into account, the additional resonant inductance can be expressed as the sum of the inductance by the air coil $L_{\rm AC}$ and the net increase of inductance by magnetic core $\Delta L_{\rm MC}$ [20]

$$L_a = L_{\rm AC} + \Delta L_{\rm MC} = \frac{10\pi\mu_o N_{\rm out}^2 a^2}{9a + 10l_A} + \frac{\mu_o \mu_r N_{\rm out}^2 w_M t_M}{l_M[1 + N_d(\mu_r - 1)]} \tag{9}$$

$$a = \sqrt{\frac{(w_A + 2d_W)(t_A + 2d_W)}{\pi}} \tag{10}$$

where μ_o is the permeability of air, μ_r is the relative permeability of core, $N_{\rm out}$ is the number of outer turns, l_A is the length of air coil, w_M is the width of magnetic core, t_M is the thickness of magnetic core, l_M is the length of magnetic core, N_d is the demagnetizing factor, w_A is the width of air core, d_W is the diameter of coil, and t_A is the thickness of air core.

Fig. 8 shows the test core and the theoretical additional resonant inductance according to the number of outer turns. An EI3633 ferrite core and triple isolation wire with 0.9 mm are used. Since l_A is in proportion to $N_{\rm out}$, $L_{\rm AC}$ is in proportion to $N_{\rm out}$. However, since $\Delta L_{\rm MC}$ is larger than $L_{\rm AC}$ and it is in proportion to $N_{\rm out}^2$, the total additional resonant inductance $L_{\rm total}$ is in almost proportion to $N_{\rm out}^2$. As mentioned in the previous section, L_a has to be larger value than 11 μH to achieve ZVS

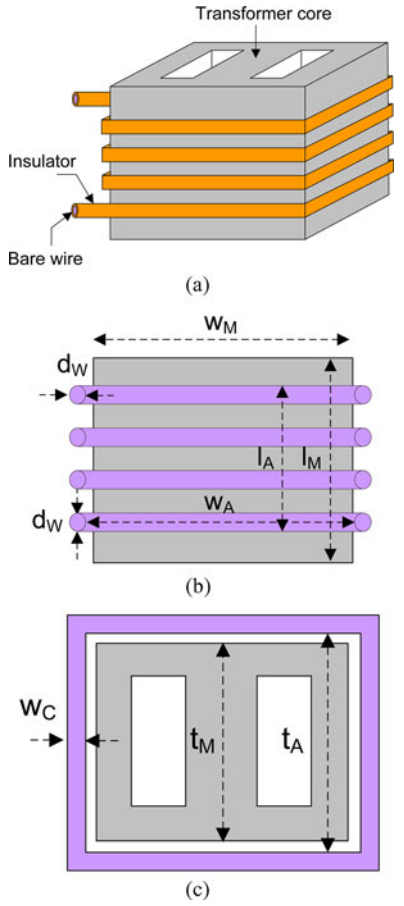

Fig. 7. Structure of L_a by the proposed winding method. (a) Overall view. (b) Front view. (c) Top view.

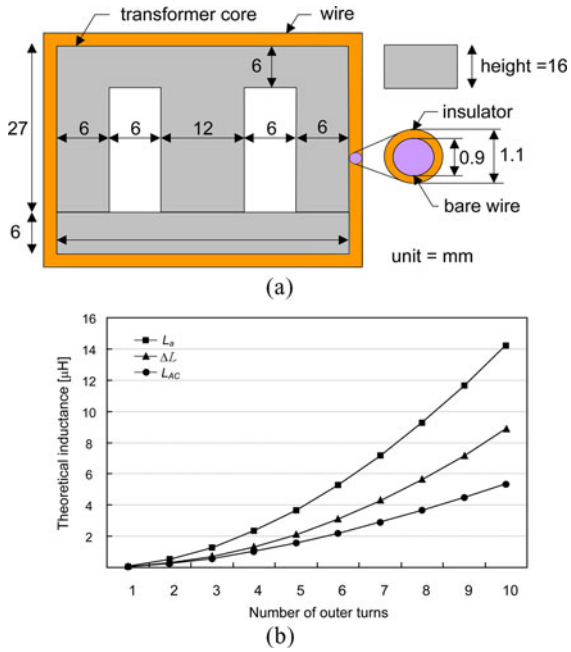

Fig. 8. Test core and theoretical additional resonant inductance. (a) Test core. (b) Theoretical additional resonant inductance.

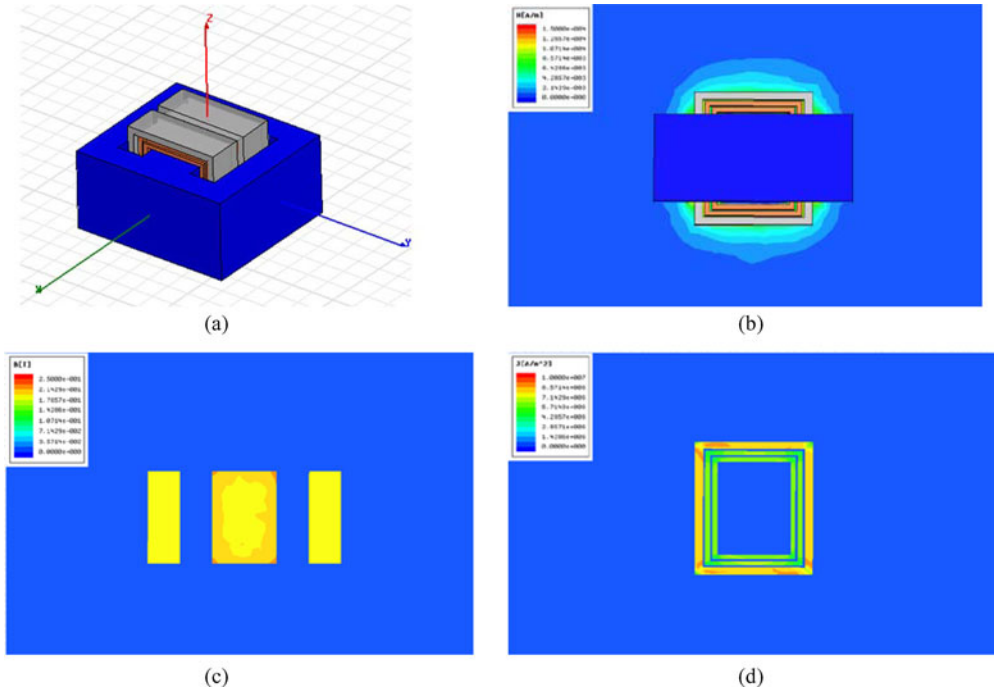

Fig. 9. FEM simulation results of conventional transformer. (a) 3-D model. (b) Magnetic field. (c) Magnetic flux density. (d) Current density.

operation above half-load conditions. Thus, nine outer turns are selected.

C. Finite Element Method (FEM) Simulation

Since the additional resonant inductor of proposed transformer works as a rod inductor, high stray flux occurs around magnetic core compared to the conventional resonant inductor using extra magnetic component. This high stray flux could cause heat problems on metallic components and high copper loss on primary/secondary wire.

Figs. 9 and 10 show FEM simulation results of the conventional transformer and the proposed transformer when the peak primary current (5.1 A) flows. As shown in Fig. 9(b), the conventional transformer has stray magnetic flux above/below the magnetic core by the coupled coefficient between primary and secondary. On the other hand, the proposed transformer has additional stray flux around the magnetic core due to the outer winding. Therefore, metallic components, such as iron case and heat sink, should keep a distance from the proposed transformer.

Figs. 9(c) and 10(c) show the magnetic flux density in the transformer core. Since the additional resonant inductor works as a rod inductor, the magnetic flux density by outer winding can be calculated using magnetic filed in the air. From Fig. 10(b), it can be seen that outer winding makes only several millitesla. Therefore, magnetic flux density by outer winding can be neglected.

Figs. 9(d) and 10(d) show the current density using eddy current analysis. As mentioned earlier, magnetic flux by outer winding has very small values. In addition, most magnetic flux flows along the outer winding. Therefore, high copper loss due to fringing flux, which often occurs in the gapped transformer, does not occur in the proposed transformer.

D. Size and Power Loss Comparison

Table I shows the specification of the transformer and additional resonant inductor. For the proposed transformer, EI3633 (volume = 16848 mm^3 and area product = 13608 mm^2) ferrite core and nine outer turns are used. For the conventional PSFB converter, EI3633 ferrite core and CS172026 (volume = 960 mm^3, area product = 1340 mm^2, and outer diameter = 17.2 mm) sendust powder resonant inductor, respectively.

Table II shows the calculated power losses of additional resonant inductor. For copper losses, they are calculated using harmonic rms values of primary current, ac resistance considering eddy current loss [21]. For conventional additional resonant inductor, it has 1.137 W core loss and 0.796 W copper loss when nonsinusoidal excitation is not considered. However, when nonsinusoidal excitation is considered, its core loss is dramatically increased to 7.503 W due to high *dB*/*dt*. On the other hand, the proposed additional resonant inductor can have very small core loss due to the small ΔB even though it also has high *dB*/*dt*.

IV. Experimental Results

Based on design considerations, a 1200-W PSFB converter incorporated with the proposed transformer is implemented with following server power specifications: input voltage: $V_{\rm in} = 320$–400 V, output voltage: $V_o = 12$ V, switching frequency: $f_s = 86$ kHz, primary switches: M_1–M_4 = SPP20N60C3, transformer turn ratios: N_p:N_{S1}:N_{S2} = 24:1:1, magnetizing inductor: L_m = 1.7 mH, transformer's leakage inductance: $L_{\rm lkg} = 6.5$ μH, additional resonant inductor: $L_a = 11$ μH (nine outer turns), clamping diodes: D_{C1} and D_{C2} = ES1J, synchronous rectifiers: SR_1 and SR_2 = IRFB3206.3 in parallel, output inductor:

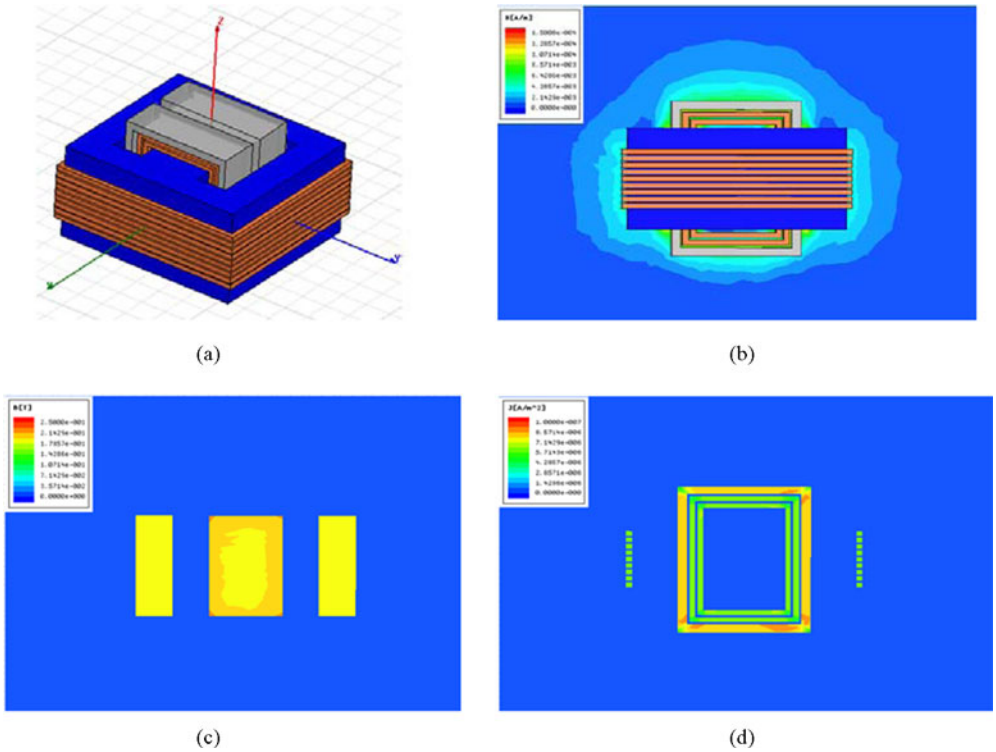

Fig. 10. FEM simulation results of proposed transformer. (a) 3-D model. (b) Magnetic field. (c) Magnetic flux density. (d) Current density.

TABLE I
SPECIFICATION OF MAGNETIC COMPONENTS

	Proposed winding method	Conventional winding method	
	Proposed transformer	Transformer	L_a
Part name	EI3633	EI3633	CS172026
Material	Ferrite	Ferrite	Sendust
κ	0.203	0.203	6.37
α	1.309	1.309	1.737
β	2.348	2.348	2.059
Volume	16848 mm^3	16848 mm^3	960 mm^3
Area Product	13608 mm^4	13608 mm^4	1340 mm^4
Number of turns	24 turns : 1 turn : 1 turn	24 turns : 1 turn : 1 turn	24 turns
Primary wire	0.9mm	0.9mm, 24 turns	0.9mm
Secondary wire	Width: 8mm, thickness: 1.5mm	Width: 8mm, thickness: 1.5mm	•
Outer wire	0.9mm, 9turns	•	•

$L_o = 1.2\ \mu$H, output capacitor: $C_o = 1650\ \mu$F, and Fan = PFB0412EHN (12 V, 6 W, r/min = 1600).

Fig. 11 shows the prototype converter and magnetic components. For the conventional PSFB converter, EI3633 (volume = 16848 mm^3) ferrite core and sendust powder core (volume = 960 mm^3) are used for transformer and additional resonant inductor, respectively. On the other hand, the proposed converter uses only EI3633 ferrite core.

Fig. 12 shows measured inductances according to $N_{\rm out}$. Since $L_{\rm lkg}$ is determined by coupling coefficient between N_p and $N_{S1,S2}$, it has same values regardless of $N_{\rm out}$. L_a is from 60 nH to 32 μH according to $N_{\rm out}$. The total resonant inductance $L_{\rm total}$ is equal to the sum of $L_{\rm lkg}$ and L_a. To achieve

TABLE II
POWER LOSS COMPARISON OF ADDITIONAL RESONANT INDUCTOR

	Proposed winding method	Conventional winding method
Core loss using SE	0.093 W	1.137 W
Core loss using MSE	0.617 W	7.503 W
Copper loss	1.542 W	0.796 W
Total power loss	2.252W	8.299 W

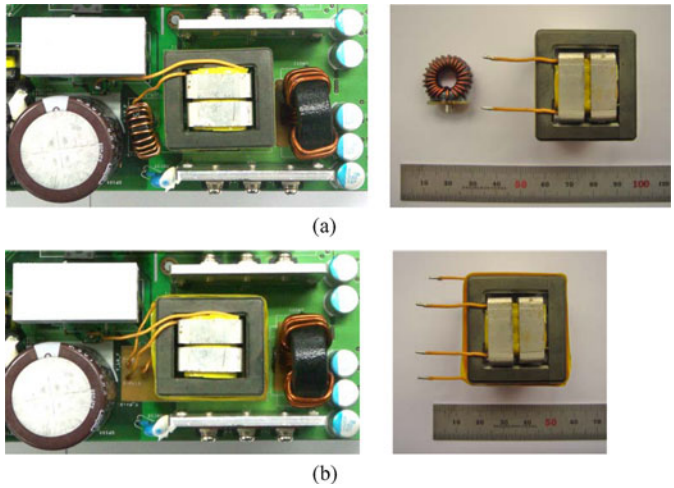

Fig. 11. Prototype PSFB converter and magnetic components. (a) Conventional PSFB converter. (b) PSFB converter incorporated with proposed transformer.

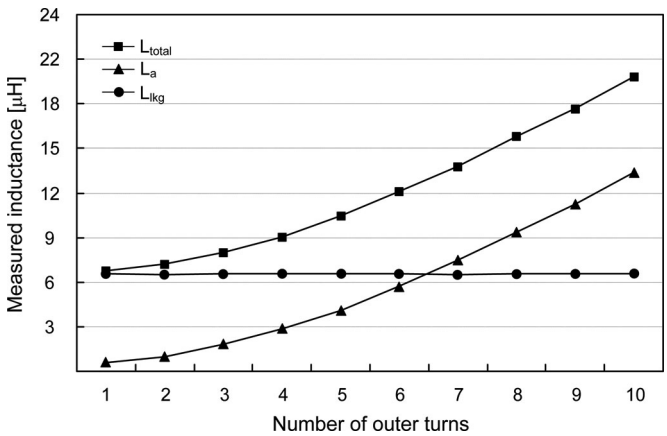

Fig. 12. Measured inductances of proposed transformer according to number of outer turns.

ZVS operation above half-load conditions, nine outer turns is selected.

Fig. 13 shows the key experimental waveforms of the PSFB converter with the proposed transformer. All waveforms well coincide with theoretical waveforms of the conventional PSFB converter with primary clamping diodes.

Fig. 14 shows the gate signals and drain-to-source voltages of all switches at half-load condition. The drain-to-source voltage reaches zero before the gate signal reaches its threshold voltage, thus ZVS operations are achieved as designed in previous section.

Fig. 15 shows the measured efficiency according to load variations. Input power is measured with the PM3000 power analyzer and output voltage is measured with digital multimeter, and output current is controlled using constant current mode of electric load. Since all parameters/devices except for the structure of the additional resonant inductor are same, the input power difference is equal to the power loss difference due to the additional resonant inductor. As shown in Fig. 15, the PSFB converter incorporated with the proposed transformer shows 0.3%–0.5% higher efficiency than the conventional PSFB converter over entire load conditions. This high efficiency is the result of the reduced core loss of L_a by adopting the proposed transformer.

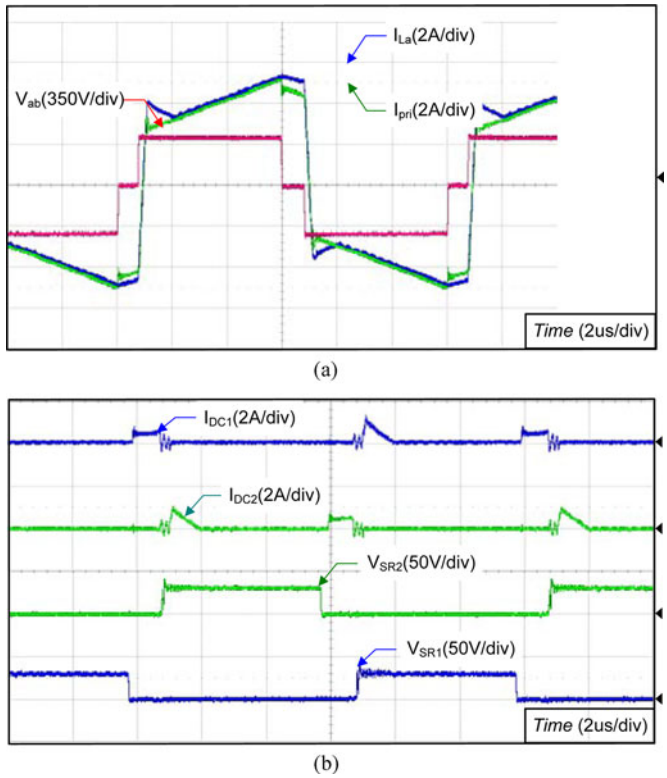

Fig. 13. Key experimental waveforms. (a) V_{ab}, I_{L_a}, and $I_{\rm pri}$. (b) I_{DC1}, I_{DC2}, $V_{\rm SR1}$, and $V_{\rm SR2}$.

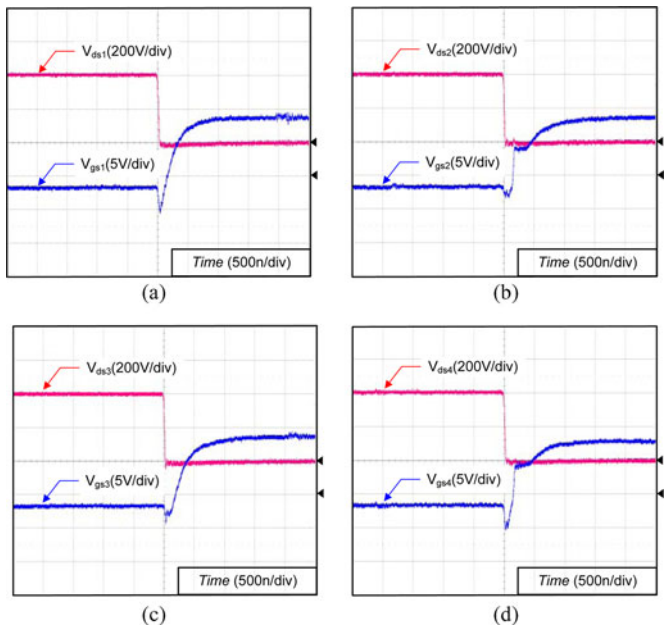

Fig. 14. Gate signals and drain-to-source voltages of all switches at half load condition. (a) V_{gs1} and V_{ds1}. (b) V_{gs2} and V_{ds2}. (c) V_{gs3} and V_{ds3}. (d) V_{gs4} and V_{ds4}.

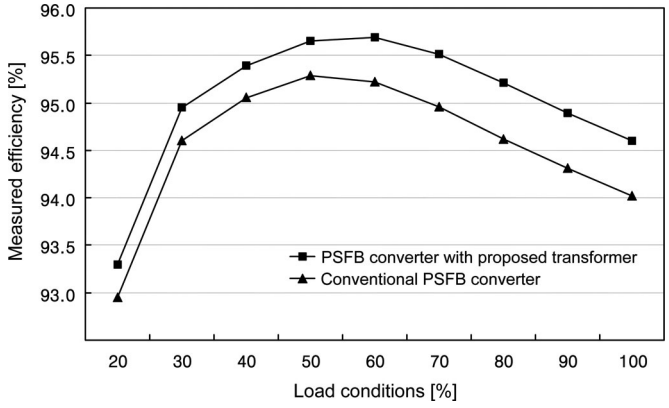

Fig. 15. Measured efficiency.

V. Conclusion

A new transformer integrated with the additional resonant inductor is proposed in this paper. The proposed transformer implements the additional resonant inductor without extra magnetic core by utilizing the outer side of transformer. As a result, it can reduce cost and core loss by the additional resonant inductor. In addition, it can adopt primary clamping diodes to reduce the voltage ringing of SRs because the additional resonant inductor and the transformer work independently. Experimental result of a 1200-W prototype dc/dc converter shows that the proposed transformer is very suitable for the conventional PSFB converter with primary clamping diodes.

References

[1] L. H. Mweene, C. A. Wright, and M. F. Schlecht, "A 1 kW 500 kHz front-end converter for a distributed power supply system," *IEEE Trans. Power Electron.*, vol. 6, no. 3, pp. 398–407, Jul. 1991.

[2] J. A. Sabate, V. Vlatkovic, R. B. Ridley, F. C. Lee, and B. H. Cho, "Design considerations for high-voltage high-power full-bridge zero-voltage-switched PWM converter," in *Proc. IEEE APEC*, 1990, pp. 275–284.

[3] H. Cha, L. Chen, R. Ding, Q. Tang, and F. Z. Peng, "An alternative energy recovery clamp circuit for full-bridge PWM converters with wide ranges of input voltage," *IEEE Trans. Power Electron.*, vol. 23, no. 6, pp. 3828–2837, Nov. 2008.

[4] C. Zhao, X. Wu, P. Meng, and Z. Qian, "Opimum design consideration and implementation of a novel synchronous recfified soft-switched phase-shift full-bridge converter for low-output voltage high-output-current applications," *IEEE Trans. Power Electron.*, vol. 243, no. 2, pp. 388–397, Feb. 2009.

[5] M. Borage, S. Tiwari, S. Bhardwj, and S. Kotaiah, "A full bridge DC-DC converter with zero voltage switching over the entire conversion ranges," *IEEE Trans. Power Electron.*, vol. 23, no. 4, pp. 1743–1750, Jul. 2008.

[6] S. Y. Lin and C. L. Chen, "Analysis and design for RCD clamped snubber used in output rectifier of phase shifted full-bridge ZVS converters," *IEEE Trans. Ind. Electron.*, vol. 45, no. 2, pp. 358–359, Apr. 1998.

[7] J. A. Sabate, V. Vlatkovic, R. B. Ridley, and F. C. Lee, "High-voltage, high-power, ZVS, full-bridge PWM converter employing an active snubber," in *Proc. IEEE APEC*, 1991, pp. 158–163.

[8] K. B. Park, C. E. Kim, G. W. Moon, and M. J. Youn, "Voltage oscillation reduction technique for phase-shift full-bridge converter," *IEEE Trans. Ind. Electron.*, vol. 54, no. 5, pp. 2779–2790, Oct. 2007.

[9] R. Redl, N. O. Sokal, and L. Balogh, "A novel soft-Switching full-bridge DC/DC converter: analysis, design considerations, and experimental results at 1.5 kW, 100 kHz," *IEEE Trans. Power Electron.*, vol. 6, no. 3, pp. 408–418, Jul. 1991.

[10] W. Chen, X. Ruan, and R. Zhang, "A novel zero-voltage-switching PWM full bridge converter," in *IEEE Trans. Power Electron.*. vol. 23, no. 2, Mar. 2008, pp. 793–801.

[11] M. K. Kazimierczuk and H. Sekiya, "Design of ac resonant inductors using area product method," in *Proc. IEEE 1st Energy Convers. Conf. Expo.*, Sep. 2009, pp. 994–1001.

[12] M. H. Sekiya and M. K. Kazimierczuk, "Design of RF-choke inductors using core geometry coefficient," in *Proc. IEEE Electr. Manuf. Coil Winding Conf.*, Sep. 2009.

[13] A. P. Van Den Bossche, D. M. Van de Sype, and V. C. Valchev, "Ferrite loss measurement and models in half bridge and full bridge waveforms," in *Proc. IEEE PESC*, 2005, pp. 1535–1539.

[14] W. A. Roshen, "A practical, accurate and very general core loss model for nonsinusoidal waveforms," *IEEE Trans. Power Electron.*, vol. 22, no. 1, pp. 30–40, Jan. 2007.

[15] J. Reinert, A. Brockmeyer, and R. W. A. A. De Concker, "Calculation of losses in ferro- and ferrimagnetic materials based on the modified Steinmetz equation," *IEEE Trans. Ind. Appl.*, vol. 37, no. 4, pp. 1055–1061, Jul./Aug. 2001.

[16] D. Lin, P. Zhou, W. N Fu, Z. Badics, and Z. J. Cendes, "A dynamic core loss model for soft ferromagnetic and power ferrite materials in transient finite element analysis," in *IEEE Trans. Magn.*. vol. 40, no. 2, Mar. 2004, pp. 1318–1321.

[17] J. Li, T. Abdallah, and C. R. Sullivan, "Improved calculation of core loss with nonsinusodial waveforms," in *Proc. IEEE IAC*, 2001, pp. 2203–2210.

[18] R. F. Soohoo, "Magnetic thin film inductors for integrated circuit applications," *IEEE Trans. Magn.*, vol. 15, no. 6, pp. 1803–1805, Nov. 1979.

[19] A. I. Pressman, *Switching Power Supply Design*, 3rd ed. New York: McGraw-Hill, 2009, pp. 356–358.

[20] D. W. Lee, K. P. Hwang, and S. X. Wang, "Fabrication and anlysis of high performance integrated solenoid inductor with magnetic core," *IEEE Trans. Magn.*, vol. 44, no. 11, pp. 4089–4095, Nov. 2008.

[21] R. W. Erickson and D. Maksimovic, *Fundamental of Power Electronics*, 2nd ed. Norwell, MA: Kluwer Academic, 2001, pp. 491–531.

Kyu-Min Cho (S'08) was born in Korea, in 1978. He received the B.S. degree from Kungpook National University, Daegul, Korea, in 2003, and the M.S. degree in the electrical engineering from the Korea Advanced Institute of Science and Technology, Daejeon, Korea, in 2003, where he is currently working toward the Ph.D. degree.

His current research interests include dc/dc converters, power-factor-correction ac/dc converters, backlight inverters of LCD TV, driver circuits of LCD TV, server power supply, and notebook adapter.

Mr. Cho is a member of the Korean Institute of Power Electronics.

Young-do Kim (S'06) was born in Korea, in 1983. He received the B.S. degree in the electrical engineering and computer science, and the M.S. degree in automobile engineering from Korea Advanced Institute of Science and Technology, Daejeon, Korea, in 2006 and 2008, respectively, where he is currently working toward the Ph D. degree.

His current research interests include dc/dc converters, ac/dc converters, and soft-switching technique

Mr. Kim is a member of the Korean Institute of Power Electronics.

In-Ho Cho (S'09) was born in Korea, in 1982. He received the B.S. degree from Han-Yang University, Seoul, Korea, in 2007, and the M.S. degree in the electrical engineering from the Korea Advanced Institute of Science and Technology, Daejeon, Korea, in 2009, where he is currently working toward the Ph.D. degree.

His current research interests include dc/dc converter, power-factor-correction (PFC) ac/dc converters, and server power system.

Mr. Cho is a member of the Korean Institute of Power Electronics.

Gun-Woo Moon (S'92–M'00) received the M.S. and Ph.D. degrees in electrical engineering from the Korea Advanced Institute of Science and Technology (KAIST), Daejeon, Korea, in 1992 and 1996, respectively.

He is currently a Professor in the Department of Electrical Engineering, KAIST. His research interests include modeling, design and control of power converters, soft-switching power converters, resonant inverters, distributed power systems, power-factor correction, electric drive systems, driver circuits of plasma display panels, and flexible ac transmission systems.

Dr. Moon is a member of the Korean Institute of Power Electronics, Korean Institute of Electrical Engineers, Korea Institute of Telematics and Electronics, Korea Institute of Illumination Electronics and Industrial Equipment, and Society for Information Display.